THE ASTROPHYSICAL JOURNAL, 378:557–564, 1991 September 10

A GASEOUS TAIL ABLATED FROM THE SUPERGIANT IRS 7 NEAR THE GALACTIC CENTER

E. SERABYN[1]
Division of Physics, Mathematics, and Astronomy, 320–47, California Institute of Technology, Pasadena, CA 91125
AND
J. H. LACY[1] AND J. M. ACHTERMANN[1]
Department of Astronomy, University of Texas, Austin, TX 78712
Received 1990 December 26; accepted 1991 March 15

ABSTRACT

A 1″ resolution map of the [Ne II] 12.8 μm emission from the M supergiant IRS 7 near the Galactic center has revealed a 5″ long ionized "plume" or "tail" of gas leaving the star, in a direction opposite to the radio point source at the Galactic center. While the stellar envelope and tail are likely ionized by the ultraviolet radiation from the Galactic center, ram pressure is more likely to be responsible for the ablation of the supergiant's mass outflow envelope. This ram pressure could arise in one of two sources: a wind from the vicinity of the Galactic center, or the drag caused by the passage of IRS 7 through an ambient medium. In the wind scenario, since the external wind and radiation which act on this star as it orbits about the Galactic center are the same agents which act on a comet orbiting about the Sun (neglecting magnetic fields), IRS 7's "tail" can be understood as the analog of a cometary tail.

Numerical calculations of the velocity field expected along the plume for both wind and drag models are reasonably consistent with the observed velocity pattern, but higher resolution observations should be able to discriminate definitively between the two. Based on the current observations, if a wind is present (which is considered more likely), the ratio of the wind force to the gravitational force on the envelope of IRS 7 is ~ 0.3, while if only a drag medium is present, the drag force to gravitational force ratio is $\lesssim 0.004$.

Subject headings: galaxies: nuclei — galaxies: The Galaxy — stars: circumstellar shells — stars: individual (IRS 7) — stars: supergiants

Near-infrared observations of the central few parsecs of our Galaxy have revealed the presence of a dense stellar cluster containing several 10^6 $M_\odot$ of stars (Becklin & Neugebauer 1968). These stars exist in an extreme environment: the stellar density, gravitational field, and ionizing luminosity are all uniquely high in the Galaxy (McGinn et al. 1989; Lacy, Townes, & Hollenbach 1982; Mezger & Wink 1986), and there is evidence for a prodigious mass outflow wind (Geballe et al. 1984, 1987; Gatley et al. 1984, 1986). Both the wind and the ultraviolet radiation apparently emanate from the innermost few arcsecond region of our Galaxy (Rieke, Rieke, & Paul 1989; Allen, Hyland, & Hillier 1990).

The brightest near-infrared source in the region is the M supergiant IRS 7 (Wollman, Smith, & Larson 1982; Lebofsky, Rieke, & Tokunaga 1982), which is thought to lie near the Galactic center because of its small projected offset ($\approx 6''$), high line-of-sight velocity (≈ -128 km s^{-1}; Sellgren et al. 1987; Rieke & Rieke 1988), and its externally ionized circumstellar envelope, seen in the [Ne II] and Brα lines, as well as via its radio free-free emission (Serabyn 1984; Rieke & Rieke 1989; Yusef-Zadeh, Morris, & Ekers 1989).

Because the [Ne II] line at 12.8 μm is bright ($I_{[\mathrm{NeII}]} \approx I_{\mathrm{H}\beta}$), and relatively unaffected by the interstellar extinction to the Galactic center ($A_{12.8\mu\mathrm{m}} \approx \frac{1}{30} A_V \approx 1$ mag), this line has often been used to study the interstellar medium in the vicinity of the Galactic center (Lacy et al. 1979, 1980; Serabyn & Lacy 1985; Serabyn et al. 1988). However, it has not previously been used to study the stellar component. Here we present a new, 1″ resolution [Ne II] map of IRS 7 and its surroundings, which reveals a rather extraordinary structure for the ionized envelope of this supergiant: the ionized emission associated with IRS 7 has the form of a 5″ long tail attached to the star. This tail has also been discovered independently with the VLA (Yusef-Zadeh & Morris 1991). As is discussed in the following, the discovery of this tail has several important implications for the nature of the interstellar medium in our Galaxy's central parsec.

2. OBSERVATIONS AND RESULTS

The observations presented here were obtained on UT 1989 July 28 on the NASA IRTF with IRSHELL, a mid-infrared cryogenic echelle spectrograph (Lacy et al. 1989b). IRSHELL uses an Si:As detector array, manufactured and loaned to us by Hughes Aircraft Co., to measure a 64 point spectrum at each of 10 positions along a focal plane slit. For these observations, the pixel spacing and slit width were both 1″. Including seeing, the resolution of the raw data is estimated to be $\sim 1\farcs6$. The data were processed with a maximum-entropy-method (MEM) deconvolution procedure, yielding a final spatial resolution of $\approx 1''$ FWHM. The processed maps resemble the raw data quite closely, however. The spectral resolution was 30 km s^{-1}, and the sampling interval 16.5 km s^{-1}. The frequency scale, set by sky emission lines, is accurate to ± 3 km s^{-1}.

Although the entire central 75″ × 90″ region of Sgr A West was mapped in the [Ne II] line, only maps of the 8″ × 9″ region surrounding IRS 7 are presented here. Mapping was done by orienting the slit N-S, and scanning the telescope in right

[1] Visiting Astronomer at the Infrared Telescope Facility, which is operated by the University of Hawaii under contract with the National Aeronautics and Space Administration.

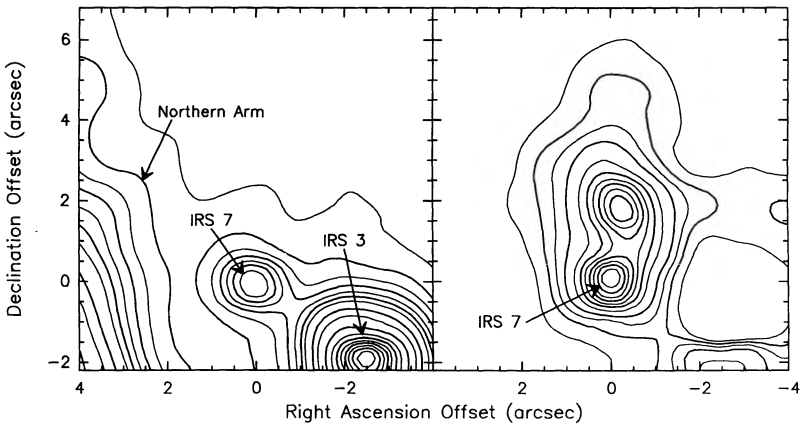

FIG. 1.—12.8 μm continuum (*left*) and [Ne II] line (*right*) maps of the IRS 7 region. The coordinates are relative to IRS 7. Contour levels for the continuum map are 0.004 to 0.036 by 0.004, then 0.045, 0.055, and 0.075 to 0.275 by 0.025 (in ergs s^{-1} cm^{-2} cm sr^{-1}), and for the line map 0.0033, 0.0067, 0.01, and 0.015 to 0.085 by 0.01 (in ergs s^{-1} cm^{-2} sr^{-1}). Because of background emission, the lowest visible contour on the continuum map is actually at the 0.012 level.

ascension. The chopping secondary was not used. Instead, background emission observed at the ends of the scans was subtracted from the spectra. Intensity calibration was obtained by measuring the emission from a blackbody inserted into the beam, checked by observations of stars, and is accurate to $\sim \pm 20\%$.

The 12.8 μm continuum map of the region surrounding IRS 7 is shown in Figure 1*a*. This map covers the velocity interval -620 to -384 km s^{-1}, which is free of line emission. The dust continuum emission from IRS 7 appears just below the center of the map, and IRS 3 to the lower right. The velocity-integrated Ne^+ emission is shown in Figure 1*b*. Six spectral channels, covering -206 to -107 km s^{-1} were summed, and the continuum map subtracted. An ionized gas component coincident with IRS 7 is clearly present, with a flux of 3×10^{-12} ergs s^{-1} cm^{-2}. Since its -120 km s^{-1} line-of-sight velocity agrees, within uncertainties, with the stellar velocity as determined from the 2.4 μm CO bandhead (-128 km s^{-1}), we conclude that the ionized emission arises in IRS 7's mass-loss envelope.

[Ne II] emission in this velocity interval also extends northward from IRS 7, with an additional flux of 3×10^{-12} ergs s^{-1} cm^{-2} arising in a northward-pointing "plume", or "tail" of gas. This plume is $\approx 5''$ long and is unresolved perpendicular to its length. The northerly direction of this tail is nearly directly opposite, to within $\pm 10°$, to that toward Sgr A*, the unique radio point source located 6″ to the south of IRS 7. This radio source is suspected to lie at, or near, the Galactic center (Lo 1989). Finally, note that the map shows some evidence that the plume is not perfectly straight.

The spectra in a north-south cut through IRS 7 reveal the velocity field along this tail. These spectra are presented in the form of a declination-velocity (δ-v) plot in Figure 2, in which the plume of gas can be followed for a distance of $\approx 5''$. From IRS 7 northward, the velocity increases from $v_{LSR} \approx -120$ km s^{-1} to ≈ -175 km s^{-1} in $\sim 3''$, with an average gradient of -18 km s^{-1} $arcsec^{-1}$. The average velocity along this section, ≈ -150 km s^{-1}, agrees quite well with the earlier large beam measurement (Serabyn 1984). Beyond 3″ from IRS 7, the velocity levels off near -180 km s^{-1}, and finally, near the plume's northernmost extremity, the velocity may drop somewhat. Because of the continuity in velocity along the plume, the match in velocities on IRS 7 itself, and the lack of other emission in this vicinity at such large negative velocities, we conclude that the tail of emission to the north of IRS 7 is intimately associated with IRS 7 and not due to an unrelated line-of-sight feature.

3. SOURCE MODELS

The observation of ionized gas associated with the red supergiant IRS 7, and its plume-like morphology, lead to two questions: (1) how is the gas ionized and (2) how is the gas ejected or swept away from the star?

We first consider, and rule out, the possibility that the gas was ejected from IRS 7 as an ionized one-sided jet. To begin with, the gas could not have been ionized when it left IRS 7. The strong CO absorption bands observed in the 2 μm spectrum of IRS 7 indicate that it is an M-type supergiant, with far too cool a spectrum to ionize the gas observed near it (Rieke & Rieke 1989). It is more difficult to rule out the possibility that the one-sided morphology of the plume is the result of its being ejected as a one-sided molecular jet which is later ionized, but outflows seen around other late-type stars are observed to be spherical or bipolar, not one-sided. It is also apparent from the observed velocity field that some force is acting on the gas after

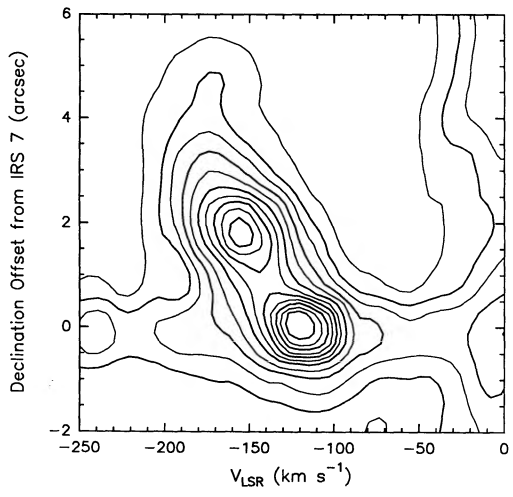

FIG. 2.—Declination-velocity diagram along the plume of emission extending northward from IRS 7. The contour levels are 0.017, 0.025, 0.033, 0.045, 0.06 to 0.2 by 0.02 (in ergs s^{-1} cm^{-2} cm sr^{-1}). The band across the figure at zero offset is due to the continuum emission from IRS 7.

it leaves the star. From these facts, we conclude that most likely the gas initially leaves IRS 7 as an approximately spherical molecular outflow, which is then ionized and carried away from the star by an external source of energy and momentum, apparently associated with Sgr A*, or a source close to its projected direction.

Threee agents seem worthy of consideration as possible causes of the ionization and/or acceleration of the gas in the plume: (1) radiation from the central stellar cluster or other central objects, (2) the drag on IRS 7's extended envelope due to its motion through the ambient interstellar medium, and (3) a wind from the vicinity of Sgr A*. We first discuss the interaction of the gas in the envelope of IRS 7 with the ionizing radiation from the central region, and later consider the effects of an ambient medium and a high velocity wind from the center.

We assume that IRS 7 loses mass at a constant rate $\dot{M}$, with a constant outflow velocity, v, resulting in an r^{-2} neutral gas density distribution, given by

$$n = \frac{\dot{M}}{4\pi m_{\rm H} v r^2}, \tag{1}$$

where $m_{\rm H}$ is the H atom mass. This assumption allows a derivation of the maximum required mass-loss rate, as any interaction with an external medium would tend to compress the outflow, and increase the emission from a given mass of gas. The problem of uniform outflow ionized by an external radiation source can be solved (e.g., Scoville & Norman 1988) by requiring that the ionization front occurs on that surface outside of which the column of recombining gas in the r^{-2} envelope is sufficient to absorb completely the ionizing photon flux, $F_{\rm UV}$, or

$$F_{\rm UV} = \alpha_{\rm B} \int_{-\infty}^{z_{\rm if}(\rho)} n_e^2 \, dz . \tag{2}$$

Here we have assumed a plane parallel ionizing flux incident along the z-axis, $z_{\rm if}(\rho)$ is the location of the ionization front as a function of the radial coordinate, ρ, perpendicular to z, $\alpha_{\rm B}$ is the case B hydrogen recombination coefficient, and n_e is the electron density. Unlike a normal H II region, the ionized gas is located outside of the front. With the density given by equation (1), this yields

$$F_{\rm UV} = \frac{\alpha_{\rm B}}{2\rho^3}\left(\frac{\dot{M}}{4\pi m_{\rm H} v}\right)^2\left[\frac{\rho z_{\rm if}(\rho)}{\rho^2 + z_{\rm if}^2(\rho)} + \tan^{-1}\left[\frac{z_{\rm if}(\rho)}{\rho}\right] + \frac{\pi}{2}\right]. \tag{3}$$

The resultant ionization front has the shape of a cylinder tapering to a rounded end. Along the line between the mass-loss star and the external radiation source, the distance from the ionization front to the star is smallest, being

$$|z_{\rm if}(0)| = \left(\frac{\alpha_{\rm B}}{3F_{\rm UV}}\right)^{1/3}\left(\frac{\dot{M}}{4\pi m_{\rm H} v}\right)^{2/3}, \tag{4}$$

and at $z = \infty$, the radius of the cylinder of neutral gas is

$$\rho_{\rm if}(\infty) = \left(\frac{3\pi}{2}\right)^{1/3} |z_{\rm if}(0)| . \tag{5}$$

The volume emission measure of the ionized gas, or volume integral of n_e^2 outside of the ionization front is given by

$$\mathrm{VEM} = \frac{3}{4}\left(\frac{\pi}{16}\frac{F_{\rm UV}}{\alpha_{\rm B}}\right)^{1/3}\left(\frac{\dot{M}}{m_{\rm H} v}\right)^{4/3}. \tag{6}$$

The emission in a collisionally excited forbidden line is proportional to the volume emission measure, as long as $n_e \ll n_c$, where n_c is the critical density for thermalization of the observed transition ($\approx 3 \times 10^5$ cm^{-3} for [Ne II]). The [Ne II] peak coincident with IRS 7 requires VEM $\approx 3.5 \times 10^{59}$ cm^{-3}, assuming an extinction to IRS 7 of 1 mag, Ne^+/H twice solar Ne/H (Lacy, Achtermann, & Bruce 1989a), and $n_e \ll n_c$.

The ionization of Sgr A West requires an ionizing luminosity, $\dot{N}_{\rm UV}$, of $\approx 2 \times 10^{50}$ photons s^{-1} (Lacy et al. 1982; Mezger & Wink 1986; rescaled for a distance of 8.5 kpc and including an estimate of the number of photons which escape the central region), and so the ionizing flux at IRS 7, assuming the radiation is emitted from sources near the center, is given by

$$F_{\rm UV} = \frac{\dot{N}_{\rm UV}}{4\pi r_{\rm pc}^2} = 1.7 \times 10^{12} r_{\rm pc}^{-2} \text{ photons cm}^{-2} \text{ s}^{-1}, \tag{7}$$

where $r_{\rm pc}$ is the distance of IRS 7 from the center in parsecs. Assuming the stellar outflow velocity is 15 km s^{-1}, a typical velocity for red giant and supergiant mass-loss winds (Knapp & Morris 1985; Knapp et al. 1989), we derive a mass-loss rate of

$$\dot{M} = 2 \times 10^{-5} r_{\rm pc}^{1/2} M_\odot \text{ yr}^{-1} . \tag{8}$$

For $r_{\rm pc} = 0.35$, which is $\sqrt{2}$ times the projected separation of IRS 7 from Sgr A* (attempting a correction for the unknown projection factor), we get $\dot{M} \approx 10^{-5}\ M_\odot$ yr^{-1}, a reasonable value for an evolved mass-loss star (Knapp & Morris 1985).

The ionization front is closest to the star at $z_{\rm if}(0) = 0.015 r_{\rm pc}$ pc, where the density is $\approx 2 \times 10^4 r_{\rm pc}^{-3/2}$ cm^{-3}, or $\approx 10^5$ cm^{-3} for $r_{\rm pc} = 0.35$. Note that if an external medium or a wind from the center contains the outflow, a smaller mass-loss rate than derived here would be required. Such a medium (or a magnetic field) is almost certainly required, since the presence of a second bright spot ~ 0.1 pc north of IRS 7 implies that the gas density is maintained at this high level even after it is swept away.

Besides ionizing the outflow, radiation would exert a pressure on it, possibly contributing to the plume nature of the observed emission. The radiation force on moderately dense ionized gas is dominated by absorption of ionizing photons by the recombining gas, and per proton is given by the product of the average momentum per photon and the absorption rate per proton, or

$$F_{\rm rad} = \left(\frac{h\nu}{c}\right)(\alpha_{\rm B} n_e) \approx 3.5 \times 10^{-34} n_e \text{ dynes} , \tag{9}$$

or $F_{\rm rad} \approx 7 \times 10^{-30} r_{\rm pc}^{-3/2}$ dynes at $z_{\rm if}(0)$. For comparison, the force of gravity on a proton is

$$F_{\rm grav} = \frac{G m_p M(r)}{r^2} \approx 2.3 \times 10^{-29} M_6 r_{\rm pc}^{-2} \text{ dynes} , \tag{10}$$

where $M_6 = M(r)/10^6\ M_\odot$, and $M(r)$ is the central mass enclosed within the galactocentric radius r. Thus, $F_{\rm rad}/F_{\rm grav} \approx 1.5 \times 10^{-5}\ n_e r_{\rm pc}^2\ M_6^{-1}$, and for $M_6 = 3$, $r_{\rm pc} = 0.35$, and $n_e = 10^5$ cm^{-3}, $F_{\rm rad}/F_{\rm grav} \approx 0.06$. Radiation pressure would quickly fall off as n_e falls away from the ionization front, however, and so would have little effect on the orbital motion of the gas unless its density is maintained at $\sim 10^5$ cm^{-3} by an external pressure. Because of this shortcoming, and because the gas density would drop too quickly for the plume to be detectable without some containment mechanism, we conclude that the

outflow from IRS 7 must also be affected either by the ambient medium through which IRS 7 moves, or by a wind from the center.

We therefore next consider the effects of a stationary ambient medium on the stellar mass-loss envelope. Such a medium could serve to contain the outflow, as well as to provide a small drag force which strips away IRS 7's envelope as it orbits about the center. Since most of the emission from an externally ionized outflow comes from near the ionization front, where the density is highest, an elongated tail with a surface brightness comparable to that near IRS 7 requires the tail density to be not much less than the density at the ionization front, $\approx 10^5$ cm^{-3}. To contain the tail at this density, the surrounding medium must have comparable pressure, or $nT \approx 10^9$ cm^{-3} K. For this medium not to be seen, it must have much lower density, and higher temperature than the observed gas (e.g., Quinn & Sussman 1985). For example, if the ambient medium were at the virial temperature of $T \approx 10^6 M_6 r_{\rm pc}^{-1}$ K $\approx 10^7$ K, a density of ≈ 100 cm^{-3} would be necessary. This type of hot rarefied medium could be the result of shock heating due to collisions between the rapidly moving thermal plasma filaments found in the central parsec. A magnetic field permeating an ambient medium could also contribute to the pressure confining the gas. A field of 1 mG, comparable to that inferred from Zeeman and polarization observations (Schwarz & Lasenby 1990; Killeen et al. 1990; Aitken et al. 1991), would provide a pressure about equal to that of the gas in the hot medium.

The rarefied medium would slow the gas on a distance scale of about $n_{\rm plume}/n_{\rm medium}$, or $\approx 10^3$ times the thickness of the compressed condensations in the plume. Assuming the plume has a diameter of 10^{-2} pc (the diameter of the ionization front, at which size the density would be $\sim 10^5$ cm^{-3}), it would be slowed in a distance of ~ 10 pc, or approximately five orbits. If it breaks up into smaller pieces, it would feel a larger drag force per unit mass. The cooling time of the hypothesized hot medium is comparable to the drag time, $\sim 10^4$–10^5 yr (Krolik, McKee, & Tarter 1981), and so the hot medium would have to be continually reheated, e.g., by continuing infall of gas.

An alternative model for the containment and acceleration of the gas is suggested by observations indicating the presence of a high-velocity wind emanating from the Galactic center (Geballe et al. 1984, 1987; Gatley et al. 1984, 1986). Geballe et al. (1987) argue that a 700 km s^{-1} wind with a mass-loss rate, $\dot{M}_{\rm gc}$, of $4 \times 10^{-3}\ M_\odot$ yr^{-1} is being emitted from an extended object or cluster of objects near IRS 16. This wind would exert a ram pressure somewhat larger than the pressure of the confining medium assumed above, with the acceleration of the gas being primarily outward. This wind does not contribute significantly to the ionization of the envelope, however, since its mechanical luminosity is only a few percent of the radiative luminosity present.

The interaction of the galactocentric high-velocity wind with the red giant stellar wind would result in a bow shock where the two winds meet. Since the shock must be stationary with respect to IRS 7, its position is given by the requirement that the momentum density, or ram pressure, in the two winds must be equal, or $n_{\rm gc} v_{\rm gc}^2 = n_{\rm rg} v_{\rm rg}^2$, where the gc and rg subscripts refer to the galactocentric and red giant wind parameters, respectively. Assuming that both winds' densities fall of quadratically with distance from their respective origins, the separation of the shock front from IRS 7 along the line toward the center is

$$z_{\rm sh} = r_{\rm pc}\left(\frac{\dot{M}_{\rm rg} v_{\rm rg}}{\dot{M}_{\rm gc} v_{\rm gc}}\right)^{1/2}, \tag{11}$$

Using the values of Geballe et al. (1987) for $\dot{M}_{\rm gc}$ and $v_{\rm gc}$, and our earlier estimate for $\dot{M}_{\rm rg}$, we find $z_{\rm sh} \approx 0.011\ r_{\rm pc}^{5/4}$ pc, which is comparable to $z_{\rm if}$. This result is not fully self-consistent, as the outflow would have $n \propto 1/r^2$ in the vicinity of the ionization front only if $z_{\rm sh} \gg z_{\rm if}$. A self-consistent calculation would consider ionization of the dense gas layer swept up by the shock and would yield a higher density in the observed gas, and a smaller $\dot{M}_{\rm rg}$.

If a high-velocity wind from the center is present, the situation IRS 7 finds itself in is then quite similar to that of a comet orbiting the Sun, with its ion tail excited by solar UV radiation and accelerated by the solar wind. It is of interest to compare the velocities in the Galactic center with those of the cometary analog. The ratio of the wind velocity to the orbital velocity is similar in the two cases, ~ 3 in the Galactic center, assuming a $\sqrt{2}$ projection correction, and ~ 10 for a comet. More disparate are the ratios of the orbital velocity to the expansion velocity of the gaseous head or envelope, ~ 100 for comets, but only ~ 10 for IRS 7. Of course, comets, also have dust tails accelerated by radiation pressure, but since we do not detect continuum radiation from IRS 7's tail, we have no information on dust in the tail. We also have no information on the interaction of magnetic fields with the tail, although they may in fact be important.

The maximum force that the galactocentric wind or the ambient medium can exert on the gas in IRS 7's tail can be estimated if we assume that the tail fully absorbs the momentum of the material it sweeps up. Assuming the tail breaks up into clumps of cross-sectional area A, each clump feels a force of $F_{\rm ram} = \rho v_{\rm rel}^2 A$, where ρ is the density of the wind or hot medium through which the clumps move at relative velocity $v_{\rm rel}$. If the galactocentric wind does not decelerate as it leaves the center, and the clumps entrained in the flow beyond IRS 7 do not change size as they leave the star, the wind force on a gas clump falls with distance from the center as r^{-2}. The ratio of wind force to gravitational force is then given by

$$\mu = \frac{F_{\rm wind}}{F_{\rm grav}} = \frac{\dot{M}_{\rm gc} v_{\rm gc}}{4\pi G m_p M(r) N_{\rm cl}}, \tag{12}$$

where $N_{\rm cl}$ is the column density of each clump. Using the wind parameters of Geballe et al. (1987), and assuming a size scale for the clumps in the flow of $z_{\rm if}$, a density of 10^5 cm^{-3} implies $\mu \lesssim 1$. The higher density implied by the self-consistent solution would reduce this limit further, while a smaller clump size would raise it. Although this estimate for μ contains large uncertainties, a comparison with the earlier radiation force calculation indicates that the estimated wind force is about a factor of 20 larger than the radiation force available.

On the other hand, if the tail is produced by the drag of a stationary ambient medium, the ratio of the drag to gravitational forces is given by

$$\beta = \frac{F_{\rm drag}}{F_{\rm grav}} = \frac{n_{\rm medium} v_{\rm orb}^2 r^2}{GM(r) N_{\rm cl}}, \tag{13}$$

where $v_{\rm orb}$ is the orbital velocity of IRS 7. With the parameters estimated earlier, $\beta \lesssim 0.1$. In this case, the radiation force

would not be negligible. Since, however, these estimated upper limits to β and μ are considerably uncertain, we estimate these parameters directly from the kinematics of the tail in the next section.

Of course, the radiation and ram pressures discussed above must affect any other extended stellar envelopes in the central parsec as well. Consequently, we have searched the larger [Ne II] maps for similar sources and have found several other compact [Ne II] line sources at velocities different from the surrounding gas flows. However, none of these correspond to known red giants or supergiants. Interestingly, it has been suggested that external photoionization of the mass-loss envelopes of giant stars also plays a role in the nuclei of active galaxies (Scoville & Norman 1988).

4. KINEMATIC MODEL CALCULATIONS

We now compare the velocity field seen along the plume to predictions based on the wind and drag scenarios. Since the observations of the tail currently consist of only a few spatial and spectral resolution elements, any comparison of the data with theoretical predictions should, at this point, be limited to the most prominent characteristics of the observed δ-v plot, such as its total velocity range and average slope.

In general terms, the velocity gradient along IRS 7's tail must be due to the different accelerations experienced by the star and the gas it has released. While the star moves under the influence of gravity alone, the gas in its tail also feels a force due to a galactocentric wind or an ambient medium. As estimated above, radiation pressure is expected to be small compared to the wind pressure. However, if no wind is present, the radial radiation force is expected to be comparable to, or even to exceed the drag force (which is opposed to the direction of motion). In addition, even in the case of a dominant wind, the force is not purely radial, since the relative motion of IRS 7 and the galactocentric wind results in an azimuthal force. Thus, a complete kinematic analysis should include both radial and azimuthal forces. Nevertheless, in this initial treatment, we consider only the effect of one force acting at a time: either a purely radial wind, or a purely tangential drag. Note that because the orbital velocity of IRS 7 is comparable to, or somewhat larger than, the velocity difference between the tail and the star, and because IRS 7's velocity of -120 km s^{-1} indicates rapid motion toward us, the stellar orbital motion must be taken into account, and the tail cannot be treated as emerging from a stationary source. It is therefore necessary to discuss IRS 7's possible orbital parameters before addressing its tail.

Although IRS 7's orbital eccentricity is unknown, the orientation of its tail provides useful information on the orientation of its orbital plane. This stems from the approximately colinear arrangement of Sgr A*, IRS 7, and its tail, which allows for four possibilities: (1) a strong wind from Sgr A* which overwhelms the gravitational force from the central mass distribution, pushing material rapidly away from the star on a line directly opposite to the center: although any inclination of the orbital plane with respect to the line-of-sight is then possible, this case is unlikely because of our earlier force estimates, and because the kinematics of the filaments in Sgr A West (Serabyn & Lacy 1985) appear to be gravitationally dominated. (2) a moderate (or weak) wind from Sgr A* or another source in its direction: the orientation of the tail, which points directly away from Sgr A*, then requires IRS 7 to follow a nearly edge-on orbit, since otherwise the tail would not point toward the source (see Fig. 3*a* for several face-on examples, to be discussed in detail below). (3) a moderate (or weak) wind from some other source, off the line toward Sgr A*, such as, e.g., IRS 16 (Simon et al. 1990; Simons, Hodapp, & Becklin 1990): since the line of the tail then does not point back to the assumed source (as in Fig. 3*a*), motion across the plane of the sky must be present, and the orbit cannot be edge-on. However, although this case is allowed, it seems unlikely, because the wind force and orbital orientation would both need to be chosen so as to result in a tail which points at a radio source which is unique in the Galaxy (Lo 1989), but not involved. (4) a distributed drag force: since the ablated material remains in IRS 7's orbital plane, the colinearity of the tail with Sgr A* again implies that the orbital plane must be seen nearly edge-on, as in case 2 (see Fig. 3*b*), if Sgr A* is near the center of the mass distribution. (If the center of the mass distribution is elsewhere, the alignment of the tail with Sgr A* must then again be ascribed to coincidence.) Since cases 2 and 4 are the most probable candidates, it seems likely that IRS 7's orbital plane is seen nearly edge-on (independent of whether a wind or drag force is present). Although this conclusion is not a certainty, for all further analysis we assume this simplest case of IRS 7 on an edge-on orbit which is oriented approximately in the N-S plane.

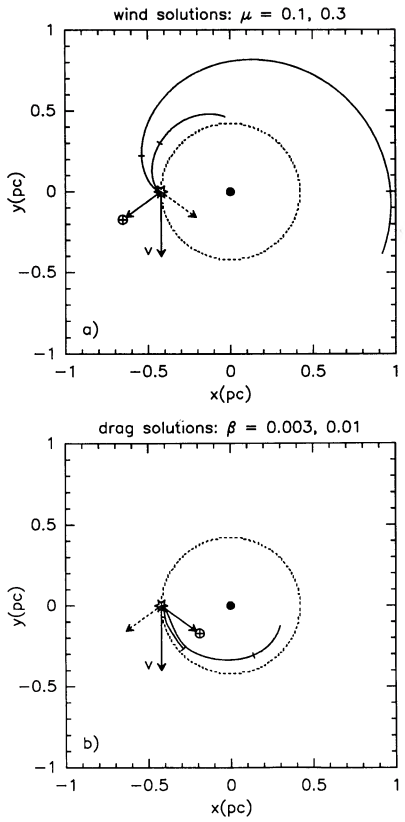

FIG. 3.—Circular orbit geometries and instantaneous tail locations for a central $4 \times 10^6\ M_\odot$ point mass. The view is perpendicular to IRS 7's orbital plane. The dotted curve shows the orbit of IRS 7 (star symbol) about the central point. The downward pointing arrow shows IRS 7's velocity vector, and the other two arrows the directions to earth allowed by IRS 7's line-of-sight velocity and projected offset from the center. The directions corresponding to the dashed arrows are ruled out by the observed tail orientation. The calculated tail locations (*solid lines*) are for (a) a wind force with $\mu = 0.1$ (short tail) and 0.3 (long tail) and (*b*) a drag force with $\beta = 0.003$ (short tail) and 0.01 (long tail). The tick marks on the tails delineate those sections of the tails which appear on the corresponding panels of Fig. 5.

The central mass distribution on which the orbit depends also needs to be defined, and for purposes of computation, we consider only the case of a central point mass, M, located at the position of Sgr A*. Assuming then that IRS 7 lies somewhere along an arbitrary (but edge-on) elliptical orbit about this center, the star's observed line-of-sight velocity, v_{los}, and its projected offset from the center, d_{proj}, can be used to constrain the orbital parameters. In the simplest case of IRS 7 on a circular orbit, there is only one value of orbital radius consistent with the observed d_{proj}, and v_{los}, for a given value of M:

$$r_0 = (GM)^{1/3}\left(\frac{d_{proj}}{v_{los}}\right)^{2/3}. \quad (14)$$

The angle which IRS 7's velocity vector makes with the line-of-sight is then $\pm\cos^{-1}(d_{proj}/r_0)$. The twofold ambiguity in angle corresponds to IRS 7 being either in front of, or behind the center. These two configurations are shown in Figure 3, which presents a face-on view of the possible orientations, for $M = 4 \times 10^6\ M_\odot$ and $d_{proj} = 0.25$ pc, for which $r_0 = 0.42$ pc.

This twofold ambiguity in observation direction can be removed with the aid of the orientation of IRS 7's tail, which, in projection, is observed to point away from the center. As can be seen in the orbital diagrams of Figure 3, which include several examples of wind- and drag-produced tails (to be discussed in detail below), only one of the two orientation vectors allows for a tail which points away from the center in projection. Thus, the orientation vectors indicated by the dashed arrows in both panels of Figure 3 are ruled out. Note that for the two types of model, the opposite orientation vector is excluded, so that in the wind model, IRS 7 is in front of the center, with a trailing tail, while in the drag case, IRS 7 is behind the center, with a leading tail.

The case of an arbitrary elliptical orbit is more complicated: for a given central mass and the two parameters defining the orbit [taken to be the eccentricity, ϵ, and r_0, where $r = r_0/(1 - \epsilon\cos\theta)$ the two remaining unknowns (θ, the azimuthal coordinate of IRS 7 along the ellipse, measured from apogalacticon, and α, the orientation of the major axis of the ellipse with respect to the line of sight) are constrained to four pairs of values. In analogy with the circular case, these four solutions are not fully independent: IRS 7's position in two of the solutions can be obtained from the other two by a reflection through the major axis of the orbit. However, again, only half of these solutions allow for tails which emerge from IRS 7 with the correct orientation, and so there are only two solutions for the angle pair (θ, α), in the case of an arbitrary ellipse. Allowing M, ϵ, and r_0 to vary then generates two families of solutions. Several representative solutions for the location of IRS 7, for $M = 4 \times 10^6\ M_\odot$, $r_0 = 0.6$ pc, and several values of ϵ, are plotted in Figures 4*a* and 4*b*. The two solutions correspond roughly to: (1) IRS 7 in the quadrant before closest approach ($90° < 180°$, with θ an increasing function of time) and (2) IRS 7 in the quadrant before apogalacticon ($270° < \theta < 360°$). In the limit of small eccentricity these two solutions become identical.

Once the parameters of IRS 7's orbit were selected, and the current orientation solved for, the wind or drag can be included, and the resultant tail calculated. The wind model was explored over all elliptical orbits accessible to IRS 7, while the drag model was only investigated for the case of circular orbits. As a simplification for these calculations, we have neglected the outflow velocity of IRS 7's envelope in comparison with the orbital and galactocentric wind velocities. Thus, a gas particle is assumed to start at the position of IRS 7, with the same velocity as the star, but after release moves under different forces. For any wind coefficient, μ, or drag coefficient, β, the location and velocity of the tail can then be calculated by following IRS 7 around the center, releasing a gas particle at each time step, and following all of these particles along their new orbits.

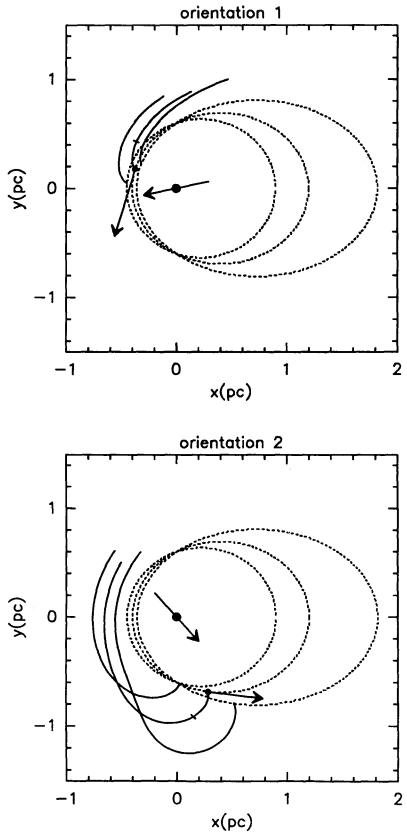

FIG. 4.—Orbital geometry and instantaneous tail locations for elliptical orbits with $M = 4 \times 10^6\ M_\odot$ and $r_0 = 0.6$ pc. The view is perpendicular to IRS 7's orbital plane. The two panels correspond to two independent families of solutions for the location of IRS 7, given the same orbital parameters. Three different elliptical orbits about the center are shown for each solution, with $\epsilon = 0.33$, 0.50 and 0.67. For the $\epsilon = 0.50$ case, the small dot shows the current location of IRS 7, and the attached arrow its velocity vector. The arrow in the center of the figures shows the direction to the observer. Also shown are the tails produced by a wind force for $\mu = 0.3$. The tick marks on several of the tails delineate those sections of the tails which appear on the corresponding panels of Fig. 5.

We begin with the wind model. Since a galactocentric wind implies an outward radial force, a simple "reduced gravity" formalism can be employed (e.g., Wurm 1963). As equation (12) indicates, a central point mass in conjunction with a constant velocity wind implies a radius-independent μ. Since this is equivalent to a reduced central mass for the gas in the tail, this case allows for a very simple solution: the particles in the tail follow Keplerian orbits about the center in the reduced gravitational field, with parameters fixed by the location of IRS 7 along its orbit at the point of release. The new eccentricity, ϵ', is then

$$\epsilon' = \frac{\sqrt{\epsilon^2 + \mu^2 - 2\mu\epsilon\cos\theta}}{1 - \mu}, \quad (15)$$

while the new azimuthal coordinate at the point of release is given by

$$\cos\theta' = \frac{1}{\epsilon'}\left(\frac{\epsilon\cos\theta - \mu}{1-\mu}\right). \quad (16)$$

Examples of the tails calculated for circular and elliptical orbits about a $M = 4 \times 10^6\ M_\odot$ central point mass are shown in Figures 3*a* and 4, respectively. In Figure 3*a*, tails for both $\mu = 0.1$ and 0.3 are shown, for one full orbit of IRS 7 about the center, while in Figure 4, tails are shown for several eccentricities, for a fixed μ of 0.3 (beginning the calculations at the orbit's maximum radius). The tails for the two families of solutions for the location of IRS 7 are shown separately in the two panels. Note that in no case shown do the tails point directly away from the center in these face-on views. This only occurs if we rotate the orbital planes to be close to edge-on, or in the limit of a very large wind force.

The final step was to project the tail's location and velocity solutions to the correct viewing angle, in order to compare with the observations. A large number of models were computed, for $M_6 = 1$, 2, 4 and 6; $\epsilon = 0$, 0.33, 0.50 and 0.67; $r_0 = 0.3$, 0.6, 0.9 and 1.2 pc (where allowed), and μ ranging from 0.01 to ~ 1. Figure 5 shows a selection of the results superposed on the observed $\delta - v$ plot. The top row of panels show the results with IRS 7 on a circular orbit, and the next two are for orbits with $\epsilon = 0.5$. The orbital parameters for the latter two rows are identical, and differ only in IRS 7's position along the orbit, the second row corresponding to solution 1 of Figure 4*a* for IRS 7's location, and the third row to solution 2. The wind force increases left to right across the panels, and every panel shows results for several values of M.

As seen in Figure 5, the model results do not depend significantly on the orbital eccentricity over the range explored, but depend strongly on M and μ. The primary results evident in the top three rows of the figure are (1) low-wind models ($\mu \leq 0.1$) do not attain the velocities seen along the tail, (2) high-wind models ($\mu \geq 0.5$) exceed the velocities and gradients seen, (3) intermediate-wind models ($\mu \approx 0.3$) provide an acceptable fit, given the low resolution of the observations, and (4) for elliptical orbits, solution 2 yields better fits than solution 1 (although solution 1 can reach the velocities seen, the entire velocity shift occurs within an arcsecond of IRS 7, with only a small velocity gradient thereafter). Conclusion 4 implies that IRS 7 is on its way out from the center. The initial rapid velocity gradient seen near IRS 7 in several of the more acceptable models (e.g., for $\mu = 0.3$ in the first and third rows) may be

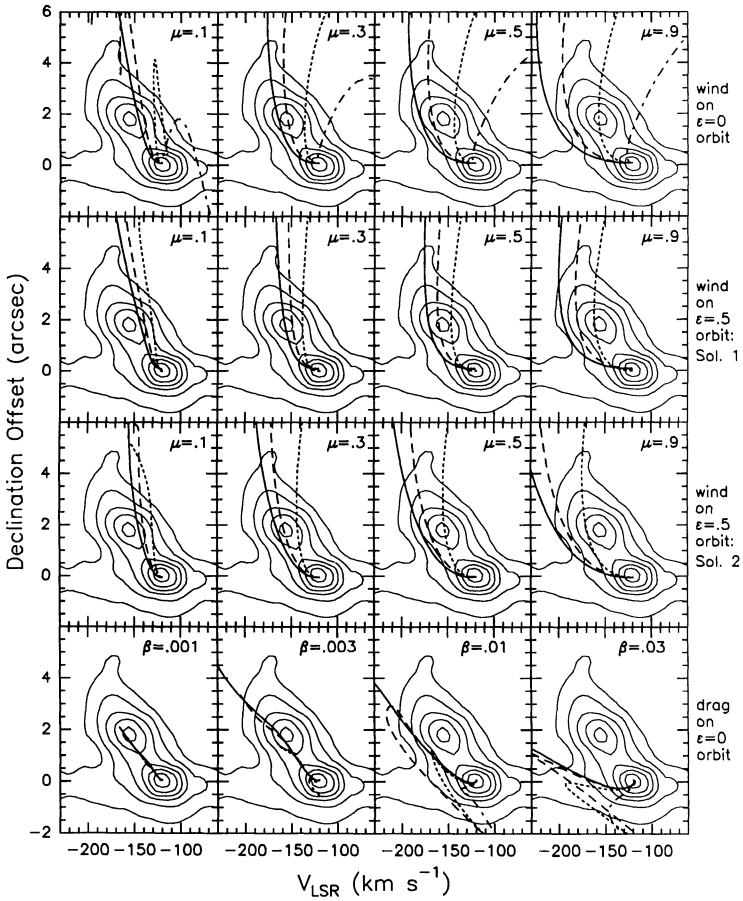

FIG. 5.—Superposition of model position-velocity curves on the observed δ–v plot. The top three rows show series of wind models, while the bottom row shows a series of drag models. For the top and bottom rows, IRS 7 is assumed to be following a circular orbit, with the geometry indicated in Fig. 3. The middle two rows assume IRS 7 is on an elliptical orbit with $\epsilon = 0.5$. Rows 2 and 3 correspond to the two families of solutions indicated schematically in Figs. 4*a* and 4*b*, respectively. Each panel shows curves for a number of central point masses: *solid curve*: $M = 6$, *dashed curve*: $M = 4$, *dotted curve*: $M = 2$, and *dash-dotted curve*: $M = 1$ (in units of $10^6\ M_\odot$). The assumed force ratio, μ (wind force to gravitational force), or β (drag force to gravitational force), is given in the upper right corner of each panel.

masked by insufficient resolution in the observations, but might also be mitigated by the wind only slowly gaining in effectiveness as the entrained clumps break up.

Intriguingly, the most acceptable solutions occur for the higher end of the explored central mass range: $M \approx 4$–6×10^6 $M_\odot$. Since a mass distribution which consists only of an r^{-2} stellar cluster would only contain $\sim 10^6$ $M_\odot$ inside of a third of a parsec (Serabyn & Lacy 1985), the approximate size of IRS 7's orbit, such a mass distribution would likely not be able to reproduce the velocities seen along IRS 7's tail.

We now turn to the drag models. These were only carried out assuming a circular orbit for IRS 7. To generate the tail, a drag force per unit mass of $-\beta v^2/r_0$ was added to the equations of motion of the released gas particles. The radial and azimuthal equations of motion were then integrated as a function of time to follow an individual particle. Finally, as in the wind case, particles were released at regular time steps along IRS 7's orbit, and the ensemble followed to generate the instantaneous tail location and velocity.

The tail locations for two values of the drag ratio β are shown in Figure 3*b*, where it can be seen that the tail now leads IRS 7, and IRS 7 is behind the center, both the reverse of the wind case. The tails shown were generated in two full orbits of IRS 7 about the center. The corresponding $\delta - v$ models are shown in the bottom row of Figure 5. For low enough $\beta (\lesssim 0.004)$ these models are better than are the wind models at producing the correct velocity gradient very close to IRS 7. However, this low drag force implies that the observed gas departs only slowly from the initial stellar orbit, and so a long time is required for the gas to diverge significantly from the star ($\gtrsim$ an orbital period). Although the gas must be kept confined for this length of time, this could result naturally from the small ratio of velocity dispersion to orbital velocity. There does seem to be the problem that at distances greater than 2″–3″ from the center, the predicted velocities keep growing, while the observed ones level off. However, it may be possible to cure this problem by putting IRS 7 on a more eccentric orbit, and so we cannot rule this model out yet.

5. SUMMARY

We have detected a tail of ionized gas leaving the M supergiant IRS 7, which, within $\pm 10°$, points directly away from the radio point source Sgr A* at the Galactic center. The ionization of the stellar envelope and tail are most likely caused by the radiation emerging from the Galactic center. On the other hand, ram pressure can explain the ablation of material from the stellar envelope, with two different sources for the pressure apparently viable: a wind from the galactic center, and the drag provided by an ambient interstellar medium. Independent of which of these two origins for the external pressure is correct, it is clear that the existence of a gaseous tail which has been ablated from the stellar envelope indicates that the bulk of the central parsec of the Galaxy must be filled with a high-pressure, low-density medium.

Both the wind and drag scenarios are consistent with the tail's projected orientation, and both are also capable of reproducing some of the main features of the velocity curve observed along this gas tail. Model calculations yield reasonable values for $F_{\rm wind}/F_{\rm grav}$ and $F_{\rm drag}/F_{\rm grav}$: 0.3 and $\lesssim 0.004$, respectively. If the tail is wind generated, the situation of IRS 7 is analogous to that of a comet orbiting about the Sun, in that both are exposed to an external radiation flux and a wind emanating from the central region. Kinematic modeling of this case indicates that IRS 7 is then in front of the center and has a trailing tail. On the other hand, if the tail is drag generated, IRS 7 is behind the center and has a leading tail. The long time scale required for the formation of the drag tail leads us to favor the wind-generation mechanism, but higher spectral resolution observations of the velocity field along the tail, combined with further modeling, should be capable of definitively discriminating between the two models.

We would like to thank the IRTF staff for assistance with the observations, and S. Phinney for helpful discussions. We also acknowledge support from NSF grants AST88-15132 and AST88-19452, and the Texas Advanced Program Research Grant No. 4574.

REFERENCES

Aitken, D. K., Gezari, D., Smith, C. H., McCaughrean, M., & Roche, P. F. 1991, preprint
Allen, D. A., Hyland, A. R., & Hillier, D. J. 1990, MNRAS, 244, 706
Becklin, E. E., & Neugebauer, G. 1968, ApJ, 151, 145
Gatley, I., Jones, T. J., Hyland, A. R., Beattie, D. H., & Lee, T. J. 1984, MNRAS, 210, 565
Gatley, I., Jones, T. J., Hyland, A. R., Wade, R., Geballe, T. R., & Krisciunas, K. 1986, MNRAS, 222, 299
Geballe, T. R., Krisciunas, K., Lee, T. J., Gatley, I., Wade, R., Duncan, W. D., Garden, R., & Becklin, E. E. 1984, ApJ, 284, 118
Geballe, T. R., Wade, R., Krisciunas, K., Gatley, I., & Bird, M. C. 1987, ApJ, 320, 562
Killeen, N. E. B., Lo, K. Y., Sault, R. J., & Crutcher, R. M. 1990, in IAU Symp. 140, Galactic and Intergalactic Magnetic Fields, ed. R. Beck, P. P. Kronberg and R. Wielebinski (Dordrecht: Reidel), p. 382.
Knapp, G. R., & Morris, M. 1985, ApJ, 292, 640
Knapp, G. R., Sutin, B. M., Phillips, T. G., Ellison, B. N., Keene, J. B., Leighton, R. B., Masson, C. R., Steiger, W., Veidt, B., & Young, K. 1989, ApJ, 336, 822
Krolik, J. H., McKee, C. F., & Tarter, C. B. 1981, ApJ, 249, 422
Lacy, J. H., Achtermann, J. M., & Bruce, D. E. 1989a, in IAU Symp. 136, The Center of the Galaxy, ed. M. Morris (Dordrecht: Reidel), p. 523
Lacy, J. H., Achtermann, J. M., Bruce, D. E., Lester, D. F., Arens, J. F., Peck, M. C., & Gaalema, S. D. 1989b, PASP, 101, 1166
Lacy, J. H., Bass, F., Townes, C. H., & Geballe, T. R. 1979, ApJ, 227, L17
Lacy, J. H., Townes, C. H., Geballe, T. R., & Hollenbach, D. J. 1980, ApJ, 241, 132
Lacy, J. H., Townes, C. H., & Hollenbach, D. J. 1982, ApJ, 262, 120
Lebofsky, M. J., Rieke, G. H., & Tokunaga, A. T. 1982, ApJ, 263, 736
Lo, K. Y. 1989, in IAU Symp. 136, The Center of the Galaxy (Dordrecht: Reidel), p. 527
McGinn, M. T., Sellgren, K., Becklin, E. E., & Hall, D. N. B. 1989, ApJ, 338, 824
Mezger, P. G., and Wink, J. E. 1986, A&A, 157, 252
Quinn, P. J., & Sussman, G. J. 1985, ApJ, 288, 377
Rieke, G. H., & Rieke, M. J. 1988, ApJ, 330, L33
———. 1989, ApJ, 344, L5
Rieke, G. H., Rieke, M. J., & Paul, A. E. 1989, ApJ, 336, 752
Schwarz, U. J., & Lasenby, J. 1990, in IAU Symp. 140, Galactic and Intergalactic Magnetic Fields, ed. R. Beck, P. P. Kronberg & R. Wielebinski (Dordrecht: Reidel), p. 383
Scoville, N., & Norman, C. 1988, ApJ, 332, 163
Sellgren, K., Hall, D. N. B., Kleinmann, S. G., & Scoville, N. Z. 1987, ApJ, 317, 881
Serabyn, E. 1984, Ph.D. thesis, University of California, Berkeley
Serabyn, E., & Lacy, J. H. 1985, ApJ, 293, 445
Serabyn, E., Lacy, J. H., Townes, C. H., & Bharat, R. 1988, ApJ, 241, 132
Simon, M., Chen, W. P., Forrest, W. J., Garnett, J. D., Longmore, A. J., Gauer, T., & Dixon, R. I. 1990, ApJ, 360, 95
Simons, D. A., Hodapp, K. W., & Becklin, E. E. 1990, ApJ, 360, 106
Wollman, E. R., Smith, H. A., & Larson, H. P. 1982, ApJ, 258, 506
Wurm, K. 1963, in The Moon, Meteorites, and Comets, ed. B. M. Middlehurst & G. P. Kuiper (Chicago: Univ. of Chicago Press), p. 573
Yusef-Zadeh, F., Morris, M., & Ekers, R. 1989, in IAU Symp. 136, The Center of the Galaxy, ed. M. Morris (Dordrecht: Reidel), p. 443
Yusef-Zadeh, F., & Morris, M. 1991, ApJL, in press